Geophysical Research Letters

RESEARCH LETTER
10.1029/2024GL109143

The Longwave Cloud-Radiative Feedback in Tropical Waves Derived by Different Precipitation Data Sets

Wei-Ting Hsiao[1] and **Eric D. Maloney**[1]

[1]Department of Atmospheric Science, Colorado State University, Fort Collins, CO, USA

Key Points:

- The updated Global Precipitation Climatology Project (GPCP) precipitation product has more frequent high rain rates, yielding a weaker longwave radiative feedback
- The updated radiative feedback supports less moistening of the Madden-Julian oscillation, but imposes stronger planetary scale selection
- The phase relationship between precipitation and thermodynamic fields in eastward-propagating tropical waves are sensitive to GPCP versions

Supporting Information:

Supporting Information may be found in the online version of this article.

Correspondence to:

W.-T. Hsiao,
WeiTing.Hsiao@colostate.edu

Citation:

Hsiao, W.-T., & Maloney, E. D. (2024). The longwave cloud-radiative feedback in tropical waves derived by different precipitation data sets. *Geophysical Research Letters*, *51*, e2024GL109143. https://doi.org/10.1029/2024GL109143

Received 13 SEP 2023
Accepted 20 APR 2024

Abstract Anomalous tropical longwave cloud-radiative heating of the atmosphere is generated when convective precipitation occurs, which plays an important role in the dynamics of tropical disturbances. Defining the observed cloud-radiative feedback as the reduction of top-of-atmosphere longwave radiative cooling per unit precipitation, the feedback magnitudes are sensitive to the observed precipitation data set used when comparing two versions of Global Precipitation Climatology Project, version 1.3 (GPCPv1.3) and the newer version 3.2 (GPCPv3.2). GPCPv3.2 contains larger magnitudes and variance of daily precipitation, which yields a weaker cloud-radiative feedback in tropical disturbances at all frequencies and zonal wavenumbers. Weaker cloud-radiative feedbacks occur in GPCPv3.2 at shorter zonal lengths on intraseasonal timescales, which implies a preferential growth at planetary scales for the Madden-Julian oscillation. Phase relationships between precipitation, radiative heating, and other thermodynamic variables in eastward-propagating gravity waves also change with the updated GPCPv3.2.

Plain Language Summary High-altitude, widespread anvil clouds are generated when heavy convective precipitation occurs in the tropics. These clouds are not only a passive product produced by convection, but they also can subsequently enhance convection by trapping upward infrared radiative flux emitted by the Earth, effectively heating the atmosphere. This additional radiative heating effect can induce upward motion in the tropics, supporting the convective systems by transporting more humid air from below. However, the strength of this cloud-radiative feedback is hard to estimate because global, continuous observations of surface precipitation are difficult to derive. In this study, the strength of the radiative feedback is calculated using the same product of observed radiative heating against two different observational precipitation products. A newer improved precipitation product yields much weaker radiative feedback strengths for all types of tropical weather systems. In addition, cloud-radiative heating is found to substantially lag behind precipitation in certain fast, eastward-propagating tropical rainfall systems in the newer precipitation product, unlike the older one. Why such a lag exists is unclear. The discrepancy of the estimation of cloud-radiative feedback strengths and properties in the older versus the newer precipitation products indicates that our understanding of mechanisms supporting tropical disturbances is still incomplete.

1. Introduction

Tropical disturbances affect global extreme weather and the hydrological cycles through their moist dynamics and associated teleconnections (e.g., Frank & Roundy, 2006; Ferrett et al., 2020; Hsiao, Barnes, et al., 2022; Maloney & Hartmann, 2000; Tseng et al., 2018). Convective systems and cloudiness are commonly coupled with tropical equatorial waves (Takayabu, 1994; Wheeler & Kiladis, 1999), and the longwave cloud-radiative feedback generated by convective clouds serves as an important mechanism modifying the development of these waves. In the Madden-Julian oscillation (MJO), the presence of convective clouds traps more longwave radiation in precipitating regions, imposing an anomalous heating effect on the atmosphere (Del Genio & Chen, 2015; Johnson & Ciesielski, 2000; Johnson et al., 2015; Lin & Mapes, 2004; Ma & Kuang, 2011). The radiative heating enhances upward velocity near the precipitation maximum, consistent with weak-temperature-gradient theory, which helps moisten the atmosphere and destabilize the MJO (Adames & Kim, 2016; Andersen & Kuang, 2012; Benedict et al., 2020; Chikira, 2014; Crueger & Stevens, 2015; Hu & Randall, 1994; M.-I. Lee et al., 2001; Raymond, 2001; A. Sobel et al., 2014; A. Sobel & Maloney, 2012; Wolding & Maloney, 2015; Zurovac-Jevtić et al., 2006). Longwave cloud-radiative feedbacks have also been suggested to support tropical cyclones (Ruppert et al., 2020), and to damp modeled equatorial Kelvin waves but support equatorial Rossby waves (Andersen & Kuang, 2012; Benedict et al., 2020; Medeiros et al., 2021).

The longwave cloud-radiative feedback can be described and measured in various ways. In moisture mode theories of convectively coupled disturbances such as the MJO, the feedback is represented by an enhancement factor of column-integrated convective heating due to cloud-radiative interaction (Fuchs & Raymond, 2002; Inoue et al., 2020; Kim et al., 2015; Lin & Mapes, 2004; Raymond, 2001; A. Sobel & Maloney, 2012; Sugiyama, 2009). Prior studies have shown that the radiative feedback parameter is dependent on zonal wavelength (Adames & Kim, 2016) and precipitation magnitude (Kim et al., 2015). The feedback has been incorporated into the "effective" gross moist stability parameter that effectively reduces the efficiency of moist static energy discharge from the column in regions of convection (e.g., Bretherton & Sobel, 2002; Raymond et al., 2009; Su & David Neelin, 2002). To specify our scope, this paper focuses on the feedback defined as the proportional factor between anomalous radiative heating and precipitation.

Accurately determining the magnitude of the radiative feedback is important for developing theories and better simulations of climate variability and tropical disturbances. Cloud-radiative heating is coupled with interannual and decadal variability in their internal dynamics (e.g., Hsiao, Hwang, et al., 2022; Rädel et al., 2016). Certain moisture mode theories of the MJO rely on the presence of radiative feedbacks to help maintain the moisture field that supports MJO convection (e.g., Adames & Kim, 2016; Jiang et al., 2020; A. Sobel & Maloney, 2012; Zhang et al., 2020). However, estimating the longwave cloud-radiative feedback using observations is difficult. Accurate observations of outgoing longwave radiation (OLR) are needed, which have been obtained through passive remote sensing by spaceborne satellites (Doelling et al., 2016; M.-I. Lee et al., 2001; Liebmann & Smith, 1996). In contrast, obtaining accurate global, continuous observations of surface precipitation are challenging due to scarce in-situ observations and large uncertainties in satellite retrievals, especially in oceanic regions that occupy the majority of area in the tropics (e.g., Bolvin et al., 2021; Prakash & Gairola, 2014; Prakash et al., 2013; Prigent, 2010).

In this paper, we examine the sensitivity of the longwave cloud-radiative feedback using two versions of Global Precipitation Climatology Project (GPCP) products and the same OLR data set, including comparisons to ground-based radar observations. Global climate-quality gridded precipitation products have been extensively used in studies of large-scale tropical systems and climate, especially for theoretical studies to determine model feedback parameters. While earlier versions of precipitation data sets (e.g., Xie & Arkin, 1997, GPCPv1.3) rely on passive remote sensing of satellites, the recently updated GPCP is considered to be more accurate by including observations of active remote sensing (Section 2.1). This study examines how much the implied radiative feedback is modified by this update. We will show that while the feedback magnitudes calculated are similar by GPCPv1.3 and earlier precipitation data sets as in prior studies (Adames & Kim, 2016; Inoue et al., 2020; Kim et al., 2015; Lin & Mapes, 2004), GPCPv3.2 yields a distinctly weaker feedback.

2. Methodology

2.1. Data

Global daily precipitation products, GPCP version 1.3 (GPCPv1.3; Huffman et al., 2001) and version 3.2 (GPCPv3.2; Huffman et al., 2023), are used. The main update for GPCPv3.2 is to replace the Threshold Matched Precipitation Index with the Integrated Multi-satellite Retrievals for GPM (IMERG) product, associated with inclusion of spaceborne precipitation radar observations from the Tropical Rainfall Measuring Mission (TRMM; Kummerow et al., 1998) and the Global Precipitation Mission (GPM; Hou et al., 2014). GPCPv3.2 has been shown to outperform GPCPv1.3 in oceanic regions in frequency of occurrence of different surface rain rates (Li et al., 2023). To obtain the non-dimensional radiative feedback, precipitation rates can be represented in W m^{-2} instead of mm day^{-1} by multiplying by the latent heat of vapourization of water (L_v) and doing a unit conversion to mass using the density of water.

Negative anomalies of National Oceanic and Atmospheric Administration Interpolated OLR (NOAA OLR; Liebmann & Smith, 1996) are used as a proxy for anomalous atmospheric column-integrated radiative heating. This allows direct comparison to results of previous studies (e.g., Adames & Kim, 2016; Lin & Mapes, 2004). Two other OLR products that include satellite observations independent from those used by NOAA OLR, the NOAA Climate Data Record (CDR) of Daily OLR Version 1.2 (H.-T. Lee et al., 2007), and Clouds and the Earth's Radiant Energy System (CERES) synoptic 1-degree (SYN1deg) Edition 4.1 observed daily OLR (Doelling et al., 2016), are also used to test the sensitivity of results to the OLR product used (Figures S1–S3 in Supporting Information S1). European Centre for Medium-Range Weather Forecasts Reanalysis v5 (ERA5; Hersbach et al., 2020) is also used to inform how the radiative feedback interacts with other atmospheric fields. All data sets

above are regridded conservatively onto the 1° × 1° grid of NOAA OLR within 15°S–15°N and during 1 September 2000 to 31 August 2021 prior to all analyses.

Precipitation estimation from two ground-based radars are used for comparison to GPCP products. The Kwajalein Polarimetric S-band Weather Radar (KPOL; Schumacher & Houze, 2000) located at 167.73°E, 8.72°N on Kwajalein Atoll provides surface precipitation rate retrieved by the HIDRO algorithm (Cifelli et al., 2011). The National Center for Atmospheric Research S-band dual-polarization Doppler radar (S-Pol; S and Ka bands; Keeler et al., 2000) employed at 0.63°S, 73.10°E on Gan Island during the DYNAMO/CINDY/AMIE field campaign, referred to as S-Pol-Gan in this study, provides surface precipitation rate retrieved by a Z-R relation (Rutledge et al., 2018). Both radars provide 1-km gridded versions of daily precipitation over a scanning radius of 150 km. Data during 1 April 2014–31 December 2021 and 1 October 2011–15 January 2012 are used from KPOL and S-Pol-Gan, respectively. For direct comparison, both GPCP products and OLR are regridded onto the same grid as in the radar products, and each daily and spatial mean over the whole scanned area is used to create a time series for temporal filtering as described in the following subsection.

2.2. Signal Filtering

In Section 3.2, a 20–100 days Lanczos band-pass filter with a 101-day window is applied to precipitation and radiative heating rates to isolate signals relevant to the MJO, with further refinements by zonal wavenumber per unit circumference of the Earth (k). The associated longwave-radiative feedback is then calculated as the negative of the slope of linearly regressed OLR onto precipitation anomalies. For validation using S-Pol-Gan, the above procedure is similarly performed but using a 30–60 days filter to obtain sufficient data points given the relatively short time range of the data.

In Section 3.3, the relationship between OLR and precipitation in other parts of wavenumber-frequency ($k-\omega$) space is also examined. Following the harmonic analysis in Wheeler and Kiladis (1999), we calculate the wave-form OLR amplitude (R), precipitation amplitude (P), and the phase shift between wave-form OLR and precipitation (φ_R) in $k-\omega$ space using the procedure published by Hayashi (1971) as described in Text S1 in Supporting Information S1. The radiative feedback parameter in $k-\omega$ space, $r(k, \omega)$, is calculated at the peak of precipitation:

$$r = \frac{R\cos(\varphi_R)}{P} \tag{1}$$

Compared to estimating the feedback parameter by directly dividing R by P in spectral space (e.g., Inoue et al., 2020), a non-zero phase lag would lead to a smaller feedback parameter r.

To obtain the variability of meteorological variables of interest associated with the precipitation anomalies in certain tropical waves, their regressions onto wave-associated precipitation are calculated as described in Text S1 in Supporting Information S1. Details of statistical significance tests are described in Text S2 in Supporting Information S1.

3. Results

3.1. Differences in Precipitation and the Climatological Radiative Feedback

General differences between the two GPCP precipitation products are first examined (Figure 1). Figure 1a compares the global annual-mean precipitation between the two versions of GPCP. While their spatial patterns are qualitatively similar (Figures S1a and S1b in Supporting Information S1), GPCPv3.2 has generally higher precipitation at the locations of maximum precipitation, such as in the Indo-Pacific warm pool, the Southern Pacific Convergence Zone, and the Inter-Tropical Convergence Zone. The climatological global tropical radiative feedback is examined in Figure 1b, calculated as in Peters and Bretherton (2005) by linearly regressing OLR onto precipitation using all grid points in Figure 1a with precipitation ≥50 W m^{-2}. Although GPCPv3.2 yields slightly weaker global radiative feedback due to its generally higher annual-mean precipitation (Figure 1a), the feedback difference yielded by the two versions of GPCP is subtle (0.02).

Although the annual-mean maps of the two GPCP products are similar, their daily variability is not. Figure 1c demonstrates a very different pattern in the histogram of observed surface precipitation rates in GPCPv1.3 and v3.2, with GPCPv3.2 having more counts above 32 mm day^{-1}. A joint histogram of the two GPCP precipitation

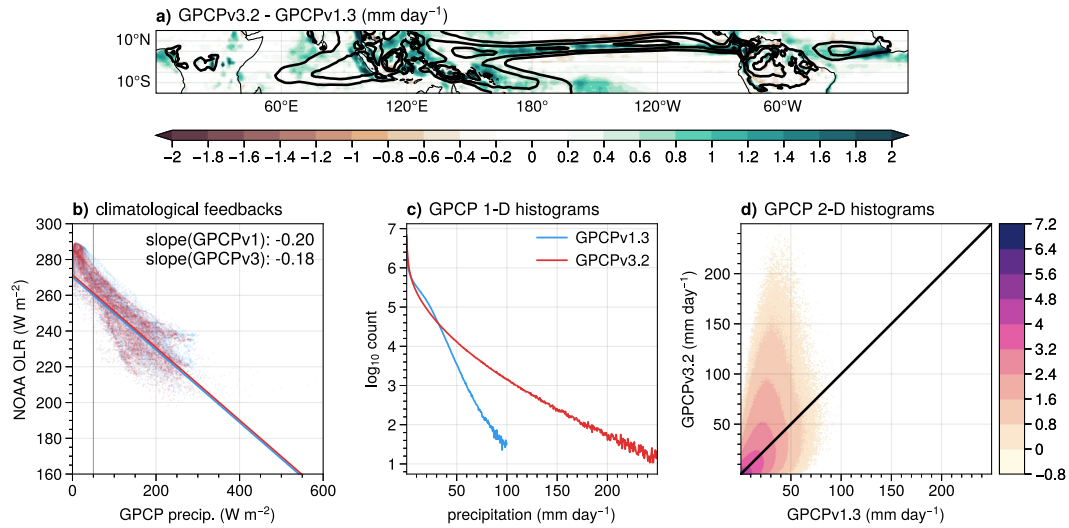

Figure 1. (a) Global annual-mean precipitation from (contour) GPCPv1.3 at 5, 7, 9 mm day^{-1} and (shading) GPCPv3.2 minus GPCPv1.3 in mm day^{-1}. (b) A scatter plot of NOAA OLR versus precipitation of (light blue) GPCPv1.3 and (dark red) GPCPv3.2 in W m^{-2} using every grid point in panel (a), and the climatological feedback calculated using data with precipitation rates above 50 W m^{-2} (vertical gray lines) annotated at the upper-right corners with the associated linear-fit lines. (c) Histograms of precipitation observations in GPCPv1.3 and v3.2 over the tropics (15°S–15°N), binned every 0.5 mm day^{-1}. (d) A joint histogram of both products with colors indicating log10 of counts, and an one-to-one black line for reference.

products shows consistent results (Figure 1d), the count distribution is skewed toward higher values of GPCPv3.2 above the one-to-one line. These differences are similar to the findings of Li et al. (2023). Increased occurrence of daily precipitation at higher values imply a weaker radiative feedback in tropical convective disturbances, which is the main focus in the following subsections.

3.2. Precipitation and Radiative Feedback in MJO

Precipitation and its radiative feedback associated with the MJO are now examined. The radiative feedback is calculated, as shown in Figure 2, for a direct comparison with Adames and Kim (2016) using 20–100 days filtered anomalies in the Indo-Pacific warm pool (60°E–180°, 15°S–15°N) where MJO activity is strongest (e.g., as in Hsiao et al., 2020). Without separating by zonal wavenumber, GPCPv1.3 yields a feedback magnitude of 0.15 (Figure 2a), whereas GPCPv3.2 yields 0.09 (Figure 2b), about half of GPCPv1.3. It is likely that the greater occurrence of heavy precipitation observed in GPCPv3.2 compared to GPCPv1.3 leads to the smaller regression slope of OLR onto precipitation on 20–100 days timescales. The updated estimate of the radiative feedback using GPCPv3.2 is smaller than those proposed in previous studies where it ranged from 0.1 to 0.2 (Adames & Kim, 2016; Bretherton & Sobel, 2002; Bretherton et al., 2005; Lin & Mapes, 2004; Peters & Bretherton, 2005).

With zonal filtering, GPCPv3.2 yields weaker feedbacks compared to GPCPv1.3 at all k (Figure 2d). On MJO spatial scales, GPCPv1.3 yields feedback magnitudes of 0.17–0.19, and GPCPv3.2 yields 0.12–0.15. The associated wave growth rates are calculated following Equation 25b and associated parameters of Adames and Kim (2016), shown in Figure 2e. While radiative feedbacks still provide a strong scale selection mechanism since longer wavelengths have higher growth rates than shorter wavelengths, the overall strength of radiative feedbacks are weaker than with GPCPv1.3. This implies that with the updated feedback parameters using GPCPv3.2, moisture mode theory would support only waves with larger zonal extent (wavelengths >7,000 km), while shorter waves are damped. Hence, the updated feedback parameter leads to a weaker theoretical MJO growth rate, but a more obvious scale selection for a planetary zonal scale over shorter zonal scales.

Further error estimation of the feedback is done using precipitation retrieved by ground-based radars. Shown in Figure 2c (also see Figures S4a–S4c in Supporting Information S1), the feedback calculated using KPOL

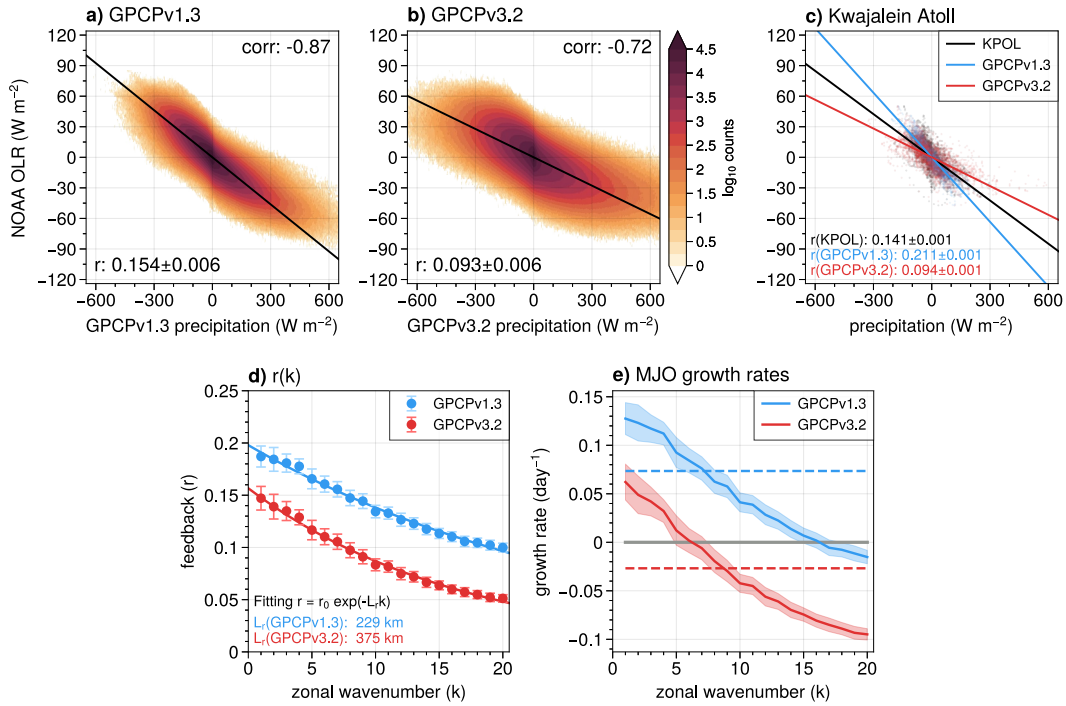

Figure 2. Bivariate histograms of 20–100 days filtered outgoing longwave radiation (OLR) and precipitation anomalies over the Indo-Pacific warm pool using (a) GPCPv1.3 and (b) GPCPv3.2. The contours are $\log_{10}$ counts, and the slope of the line shows the linear regression of OLR onto precipitation, with their 95% confidence interval (CI) and correlation coefficients (corr) annotated. (c) As in panels (a)–(b) but shows quantities located at the Kwajalein atoll (within 150-km radius from 167.73°E, 8.72°N) in a scatter plot using precipitation from (black) KPOL, (blue) GPCPv1.3, and (red) GPCPv3.2. (d) Shows the radiative feedback calculated using single zonal wavenumbers per circumference of the Earth (k) from each Global Precipitation Climatology Project version, with error bars showing 95% CI and exponential fitting lines overlaid. (e) Shows the Madden-Julian oscillation growth rate calculated as in Adames and Kim (2016) corresponding to (d), with the shading showing uncertainty using the 95% CI of r.

precipitation (0.15) lies in between those obtained by GPCPv1.3 (0.21) and v3.2 (0.09) at the Kwajalein atoll. Similar conclusions are found using S-Pol-Gan filtered by a 30–60-day window (Figures S4d–S4f in Supporting Information S1), in agreement with Ciesielski et al. (2017). Previous studies have suggested overestimated oceanic total rainfall using TRMM and IMERG (Bolvin et al., 2021; Prakash & Gairola, 2014; Prakash et al., 2013), which are products used in producing GPCPv3.2 precipitation. The above literature and evidence suggest that GPCPv3.2 may underestimate the radiative feedback of the MJO, and the actual feedback magnitude may fall between values estimated using GPCPv3.2 and GPCPv1.3.

3.3. Precipitation and Radiative Feedback in Other Tropical Waves

Next, we examine precipitation and the longwave radiative feedback over $k - \omega$ spectral space. The precipitation power spectrum of GPCPv3.2 has larger magnitudes than GPCPv1.3 over all of $k - \omega$ space, especially over where the power is already large in GPCPv1.3 (Figures 3a–3c). The radiative feedback parameter r (Figures 3d and 3e) shows a generally red noise-like distribution that is consistent with previous studies (Inoue et al., 2020; Yasunaga et al., 2019), but also with local peaks at where convectively coupled disturbances are more active, such as in regions of spectral space characterized by Kelvin waves, the $n = 1$ equatorial Rossby waves (ER), and the MJO (k of 1–5, ω of 0.01–0.05 days^{-1}). Due to the greater spectral power of GPCPv3.2, r yielded by GPCPv3.2 (using Equation 1) is overall smaller than using GPCPv1.3 (Figure 3f). Relevant to tropical wave dynamics, the increase in precipitation power from the update of GPCPv3.2 also implies a shorter convective adjustment time. This is true for all waves but especially obvious for westward-propagating tropical-disturbance -like waves (Figure S4, calculated following Yasunaga et al., 2019). This update implies a faster relaxation of moisture anomalies within the periods of these waves (a larger N_{mode} as indicated in

10.1029/2024GL109143

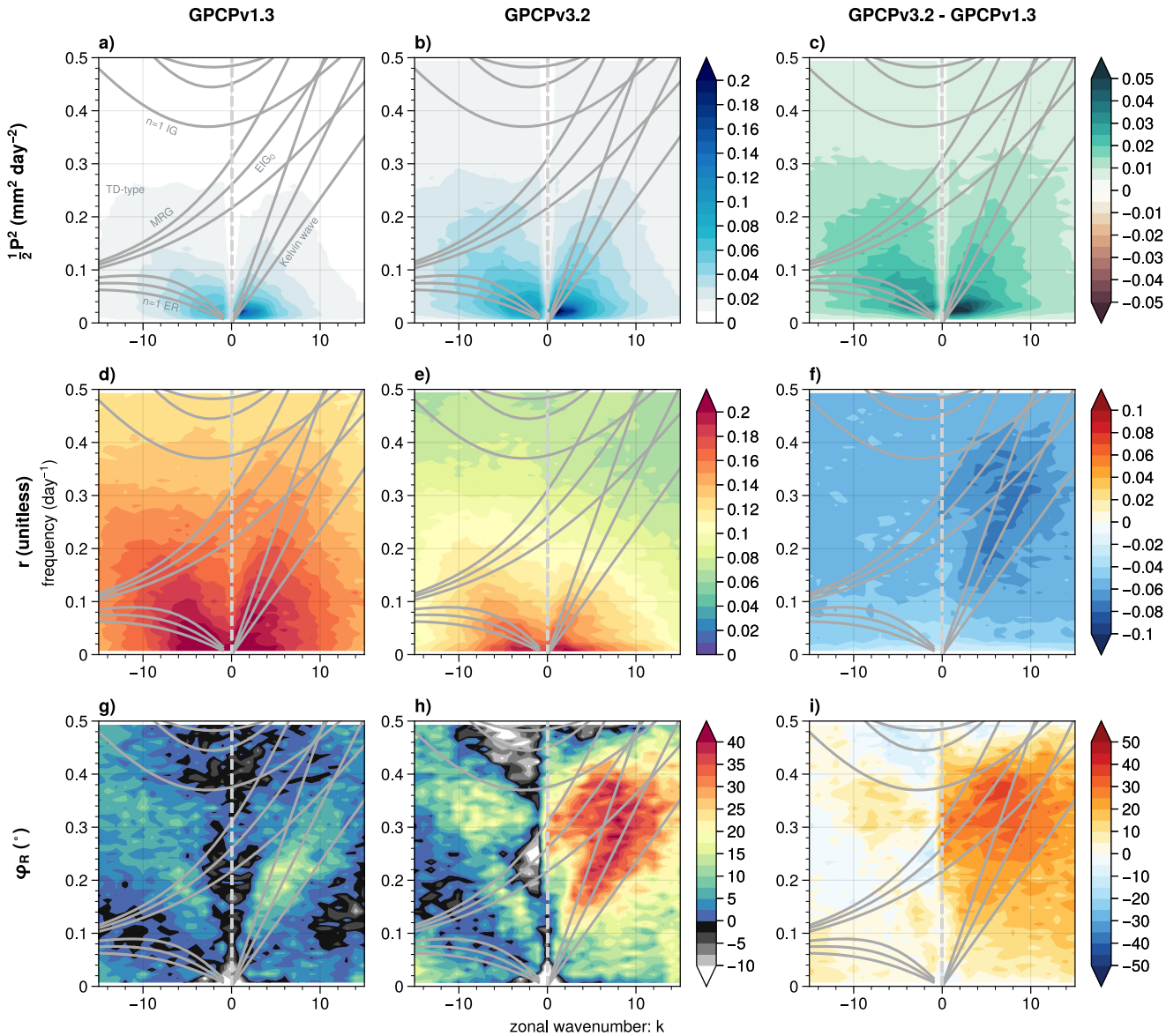

Figure 3. (a) The halved power spectra of precipitation (mm^2 day^{-2}), (d) the radiative feedback parameter *r*. (g) The phase difference between OLR and precipitation (degree). (b, e, h) shows the same quantity as (a, d, g), but yielded by GPCPv3.2, while (c, f, i) show their differences (GPCPv3.2 minus GPCPv1.3). The gray solid lines are the solutions for linear convectively coupled equatorial waves at equivalent depths of 12, 25, and 50 m, similar to those shown in Wheeler and Kiladis (1999), with associated wave types annotated in panel (a).

Adames & Maloney, 2021; Adames et al., 2019), and thus these waves might be considered more gravity wave-like instead of moisture mode-like.

The phase shift between OLR and precipitation (φ_R) shows apparent differences (Figures 3g–3i). Both products generally yield positive or small φ_R, indicating that OLR anomalies lag or are nearly in phase with precipitation. In GPCPv1.3, φ_R has a peak of 20° in Kelvin waves at frequencies near 0.2 days^{-1} (5-day period), and a similar but slightly weaker phase shift for its westward-propagating counterpart. In contrast, a large asymmetry between eastward- and westward-propagating waves is shown in φ_R using GPCPv3.2. There are distinct peaks of φ_R of ~40° in eastward-propagating $n = 0$ inertia gravity waves (EIG$_0$) and Kelvin waves, while φ_R are generally smaller than 25° for westward-propagating waves. Large φ_R in Kelvin wave and EIG$_0$ domains leads to smaller *r* compared to the conventional method that directly divides OLR by precipitation spectral amplitudes (see

10.1029/2024GL109143

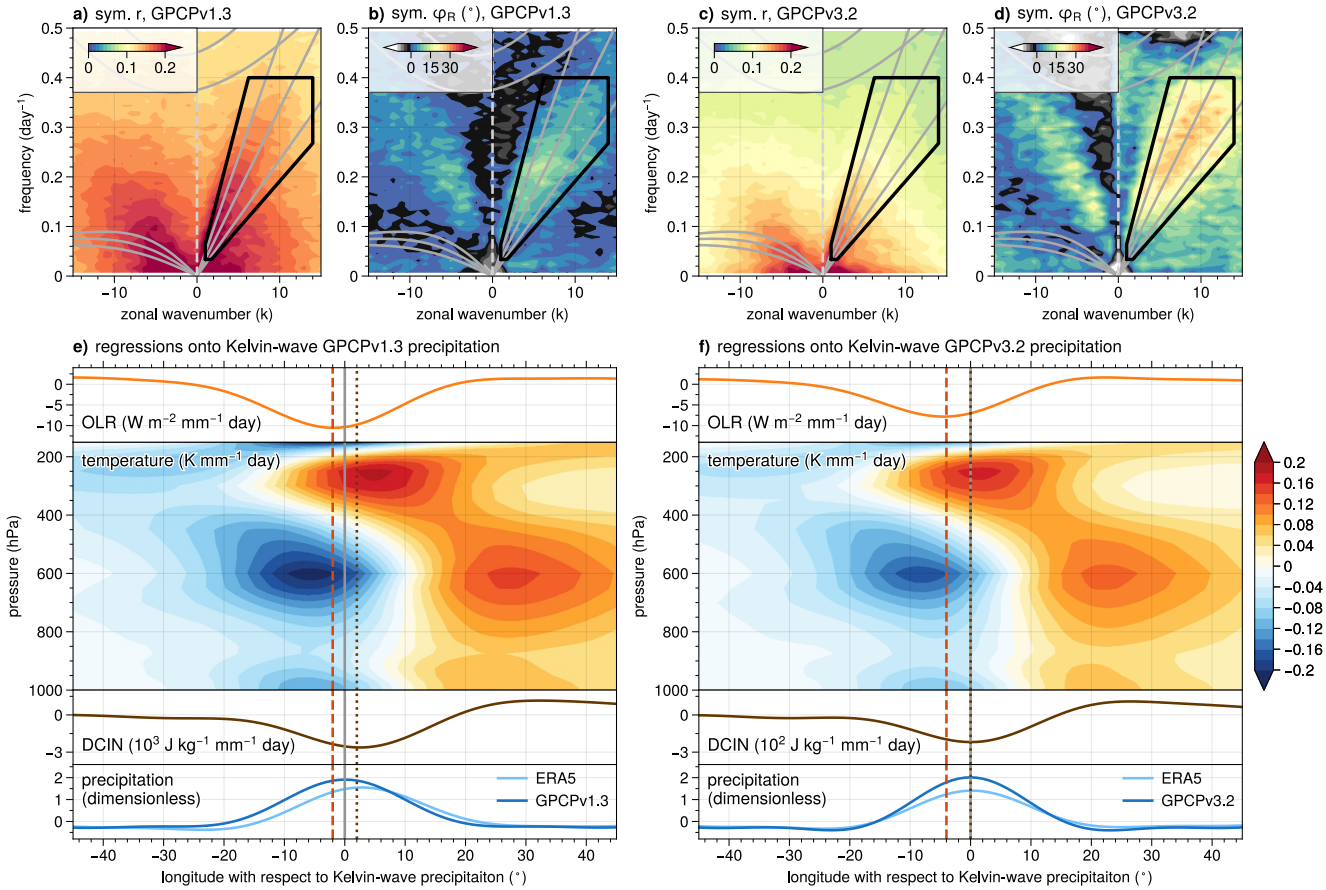

Figure 4. As in Figures 3e and 3h, but showing the latitudinally symmetric components of r and φ_R using (a–b) GPCPv1.3 and (c–d) GPCPv3.2. Areas enclosed by black lines in panels (a–d) are selected to isolate Kelvin-wave precipitation. Bottom plots show the regressions of (top row) OLR anomalies, (second row) air temperature anomalies, (third row) DCIN anomalies, and (fourth row) precipitation anomalies onto meridional-mean Kelvin-wave precipitation with lead-lag longitudes using (e) GPCPv1.3 and (f) GPCPv3.2. The longitudes of (dashed orange lines) minimum OLR, (dotted brown lines) minimum DCIN, and (solid gray lines) the center longitude of regressions are indicated in panels (e–f).

Equation 1). Why the phase shift only appears in fast eastward-propagating waves but not in westward-propagating waves is possibly related to the less top-heavy and vertically tilted structures in westward-propagating waves (Inoue et al., 2020).

Consistent with our results for eastward-propagating waves, prior studies have found vertically tilted structures in Kelvin waves and other gravity-modulated waves (Inoue et al., 2020; Kiladis et al., 2009; Mapes et al., 2006; Yasunaga & Mapes, 2012), which implies a lag in radiative heating due to the trailing high clouds produced by deep convection. However, large φ_R in Kelvin waves and small φ_R in the MJO using GPCPv3.2 are different from Najarian and Sakaeda (2023), who suggest a 45° and 0° phase difference in the MJO and Kelvin waves, respectively. As Najarian and Sakaeda (2023) also include shortwave radiation for cloud-radiative forcings, it is possible that shortwave radiation has a non-negligible effect on the phase difference. Lags of radiative heating of around 5 days behind precipitation as shown in Ciesielski et al. (2017) and Del Genio and Chen (2015) suggest an φ_R of ∼30° for the MJO (assuming a 60-day period), larger than our calculated φ_R of ∼15° in the MJO band (Figure 4h). These inconsistencies may originate from the precise way variability associated with the MJO and Kelvin waves are defined, the geographical locations of interest, and the sensitivity to not only precipitation, but also OLR data sets. For example, the magnitudes of the φ_R calculated by our method are mildly sensitive to the selection of OLR products (Figure S3 in Supporting Information S1).

If the modified values of φ_R are more realistic, do they imply different dynamical processes in Kelvin waves than using GPCPv1.3? This is examined in Figures 4e and 4f showing relevant atmospheric fields regressed onto Kelvin-wave precipitation (see Text S2 in Supporting Information S1 for method). The westward-tilted

temperature structure in the troposphere, with cold mid-tropospheric anomalies occurring during peak precipitation, is consistent with previous observations (e.g., Ma & Kuang, 2011; Wheeler et al., 2000). The minimum of regressed deep convective inhibition (DCIN; defined as the excess of saturation moist static energy in 700–800 hPa to the moist static energy in 800–1,000 hPa) is located more toward peak precipitation when using GPCPv3.2, which better supports theories in which DCIN controls the onset of deep convection associated with Kelvin waves (Fuchs et al., 2014; Raymond & Fuchs, 2007). Note that the extrema of regressed DCIN and GPCPv3.2 also coincide better with the peak of regressed ERA5 precipitation. A global climate model simulation conducted by Benedict et al. (2020) suggests that anomalous cloud-radiative heating modifies moist static energy profiles in the Kelvin waves, such that it damps the reduction in DCIN at peak Kelvin-wave precipitation. Our result yielded by GPCPv3.2 shows weaker radiative feedback, implying that such damping is weaker. The longitudinal lags between minimum DCIN and OLR are similar between the two GPCP products (5° lon yielded by GPCPv1.3, and 4° lon yielded by GPCPv3.2), so only the strength of the damping would be expected to be altered. However, it is unclear whether the distance between the damping and peak precipitation is important for wave dynamics, and a more detailed analysis is needed in future work. Similar conclusions are shown for EIG_0 in Figure S6 in Supporting Information S1.

4. Summary

The longwave cloud-radiative feedback has been hypothesized to be important for the dynamics of tropical atmospheric variability. This study examines the feedback measured by the ratio between negative OLR anomalies and surface precipitation anomalies, using two versions of the daily GPCP precipitation products versus NOAA OLR. The annual-mean tropical precipitation in the two versions of GPCP are similar, which yields similar annual-mean climatological feedback. For daily mean values, GPCPv3.2 has more frequent precipitation at higher values above 32 mm day^{-1} than in GPCPv1.3 (Figure 1b), which is associated with weaker radiative feedbacks for all types of tropical disturbances (Figure 3f).

The longwave cloud-radiative feedback has been hypothesized to explain the growth and the planetary zonal scale of the MJO under moisture mode theory (Adames & Kim, 2016; A. Sobel & Maloney, 2012). The radiative feedback associated with the MJO is calculated using 20–100 days-filtered precipitation and OLR over the Indo-Pacific warm pool (Figure 2). Without considering spatial scales, GPCPv3.2 yields a much weaker feedback (0.09) than using GPCPv1.3 (0.15). The zonal scale-dependence of the feedback is qualitatively similar using either GPCP product, in that the feedback decreases as zonal wavenumber increases, consistent with its role in preferentially supporting larger wavelengths for the MJO. When using GPCPv3.2 instead of GPCPv1.3, moisture mode theory suggests that higher wavenumbers are actually damped due to a weaker feedback, while growth only occurs at low zonal wavenumbers (wavelengths >7,000 km), suggesting a stronger growth at planetary scales for the MJO. Further comparison of the MJO radiative feedback with those yielded by ground-based radar precipitation suggests that while the feedback is overestimated in GPCPv1.3, GPCPv3.2 may underestimate the feedback. In summary, the result suggests that radiative heating provides a stronger scale-selection mechanism for the MJO than previously considered, although how much moistening is supported by radiative heating is still uncertain. This conclusion implies that other supporting feedbacks such as surface latent heat flux and frictional convergence (e.g., de Szoeke & Maloney, 2020; Hu & Randall, 1994; Maloney & Sobel, 2004; A. Sobel & Maloney, 2013; A. H. Sobel et al., 2008, 2010) might be more important than previously thought in destabilizing the MJO and possibly other tropical systems.

In $k-\omega$ spectral space, the radiative feedback parameter r calculated by either precipitation product resembles a red noise-like distribution with spectral peaks at where convectively coupled waves are more active (Figures 3d–3f). Since GPCPv3.2 has larger precipitation power than GPCPv1.3 precipitation (Figures 3a–3c), the feedback r is overall smaller (Figures 3d–3f). Interestingly, the phase shift between OLR and precipitation, φ_R, is as large as ∼40° in certain fast eastward-propagating waves (Kelvin waves and $n = 0$ eastward inertia-gravity waves) in GPCPv3.2, with GPCPv1.3 demonstrating a smaller phase shift. The minimum of DCIN coincides better with peak Kelvin-wave precipitation in GPCPv3.2. Similar conclusions are found in EIG_0 (Figure S6 in Supporting Information S1). The updated phase relations using GPCPv3.2 imply a more important role for DCIN in supporting gravity wave-associated deep convection, while the implications for radiative feedbacks are not yet clear and warrant further study.

Data Availability Statement

Data used in this manuscript can be accessed online (GPCPv1.3: https://www.ncei.noaa.gov/access/metadata/landing-page/bin/iso?id=gov.noaa.ncdc:C00999; GPCPv3.2: https://disc.gsfc.nasa.gov/datasets/GPCPDAY_3.2/summary; NOAA OLR: https://psl.noaa.gov/data/gridded/data.olrcdr.interp.html; NOAA NCEI OLR CDR daily: https://www.ncei.noaa.gov/products/climate-data-records/outgoing-longwave-radiation-daily; CERES SYN1deg: https://ceres.larc.nasa.gov/data/; ERA5: https://cds.climate.copernicus.eu/; KPOL: https://gpm-gv.gsfc.nasa.gov/Radar/index.php; S-Pol-Gan: https://orca.atmos.washington.edu/dynamo_legacy/). Available data DOI is provided (GPCPv1.3: https://doi.org/10.7289/V5RX998Z; GPCPv3.2: https://doi.org/10.5067/MEASURES/GPCP/DATA305; NOAA NCEI OLR CDR daily: https://doi.org/10.7289/V5SJ1HH2; ERA5: https://doi.org/10.24381/cds.bd0915c6). Figures in this manuscript are made by ProPlot.

Acknowledgments
This material is based upon work supported by the NASA Energy and Water Cycle Study (NEWS) Grant 80NSSC20K1105, NASA CYGNSS Grant 80NSSC21K1004, NSF Grant AGS-2217785, and NOAA CVP Grant NA22OAR4310609. The manuscript was aided by the discussion with Christian Kummerow, Nicolas Leitmann-Niimi, and Paul Stackhouse. We thank Ángel Adames-Corraliza for sharing insights on the zonal filtering for generating Figure 2, and comments from Naoko Sakaeda and one anonymous reviewer that greatly improved the manuscript.

References

Adames, Á. F., & Kim, D. (2016). The MJO as a dispersive, convectively coupled moisture wave: Theory and observations. *Journal of the Atmospheric Sciences*, *73*(3), 913–941. https://doi.org/10.1175/jas-d-15-0170.1

Adames, Á. F., Kim, D., Clark, S. K., Ming, Y., & Inoue, K. (2019). Scale analysis of moist thermodynamics in a simple model and the relationship between moisture modes and gravity waves. *Journal of the Atmospheric Sciences*, *76*(12), 3863–3881. https://doi.org/10.1175/jas-d-19-0121.1

Adames, Á. F., & Maloney, E. D. (2021). Moisture mode theory's contribution to advances in our understanding of the Madden-Julian oscillation and other tropical disturbances. *Current Climate Change Reports*, *7*(2), 72–85. https://doi.org/10.1007/s40641-021-00172-4

Andersen, J. A., & Kuang, Z. (2012). Moist static energy budget of MJO-like disturbances in the atmosphere of a zonally symmetric aquaplanet. *Journal of Climate*, *25*(8), 2782–2804. https://doi.org/10.1175/jcli-d-11-00168.1

Benedict, J. J., Medeiros, B., Clement, A. C., & Olson, J. G. (2020). Investigating the role of cloud-radiation interactions in subseasonal tropical disturbances. *Geophysical Research Letters*, *47*(9), e2019GL086817. https://doi.org/10.1029/2019gl086817

Bolvin, D. T., Huffman, G. J., Nelkin, E. J., & Tan, J. (2021). Comparison of monthly IMERG precipitation estimates with PACRAIN atoll observations. *Journal of Hydrometeorology*, *22*(7), 1745–1753. https://doi.org/10.1175/jhm-d-20-0202.1

Bretherton, C. S., Blossey, P. N., & Khairoutdinov, M. (2005). An Energy-Balance analysis of deep convective Self-Aggregation above uniform SST. *Journal of the Atmospheric Sciences*, *62*(12), 4273–4292. https://doi.org/10.1175/jas3614.1

Bretherton, C. S., & Sobel, A. H. (2002). A simple model of a convectively coupled walker circulation using the weak temperature gradient approximation. *Journal of Climate*, *15*(20), 2907–2920. https://doi.org/10.1175/1520-0442(2002)015<2907:asmoac>2.0.co;2

Chikira, M. (2014). Eastward-Propagating intraseasonal oscillation represented by Chikira–Sugiyama cumulus parameterization. Part II: Understanding moisture variation under weak temperature gradient balance. *Journal of the Atmospheric Sciences*, *71*(2), 615–639. https://doi.org/10.1175/jas-d-13-038.1

Ciesielski, P. E., Johnson, R. H., Jiang, X., Zhang, Y., & Xie, S. (2017). Relationships between radiation, clouds, and convection during DYNAMO. *Journal of Geophysical Research: Atmospheres*, *122*(5), 2529–2548. https://doi.org/10.1002/2016jd025965

Cifelli, R., Chandrasekar, V., Lim, S., Kennedy, P. C., Wang, Y., & Rutledge, S. A. (2011). A new Dual-Polarization radar rainfall algorithm: Application in Colorado precipitation events. *Journal of Atmospheric and Oceanic Technology*, *28*(3), 352–364. https://doi.org/10.1175/2010jtecha1488.1

Crueger, T., & Stevens, B. (2015). The effect of atmospheric radiative heating by clouds on the Madden-Julian oscillation. *Journal of Advances in Modeling Earth Systems*, *7*(2), 854–864. https://doi.org/10.1002/2015ms000434

Del Genio, A. D., & Chen, Y. (2015). Cloud-radiative driving of the Madden-Julian oscillation as seen by the A-Train. *Journal of Geophysical Research: Atmospheres*, *120*(11), 5344–5356. https://doi.org/10.1002/2015jd023278

de Szoeke, S. P., & Maloney, E. D. (2020). Atmospheric mixed layer convergence from observed MJO sea surface temperature anomalies. *Journal of Climate*, *33*(2), 547–558. https://doi.org/10.1175/jcli-d-19-0351.1

Doelling, D. R., Sun, M., Nguyen, L. T., Nordeen, M. L., Haney, C. O., Keyes, D. F., & Mlynczak, P. E. (2016). Advances in Geostationary-Derived longwave fluxes for the CERES synoptic (SYN1deg) product. *Journal of Atmospheric and Oceanic Technology*, *33*(3), 503–521. https://doi.org/10.1175/jtech-d-15-0147.1

Ferrett, S., Yang, G.-Y., Woolnough, S. J., Methven, J., Hodges, K., & Holloway, C. E. (2020). Linking extreme precipitation in Southeast Asia to equatorial waves. *Quarterly Journal of the Royal Meteorological Society*, *146*(727), 665–684. https://doi.org/10.1002/qj.3699

Frank, W. M., & Roundy, P. E. (2006). The role of tropical waves in tropical cyclogenesis. *Monthly Weather Review*, *134*(9), 2397–2417. https://doi.org/10.1175/mwr3204.1

Fuchs, Ž., & Raymond, D. J. (2002). Large-Scale modes of a nonrotating atmosphere with water vapor and Cloud–Radiation feedbacks. *Journal of the Atmospheric Sciences*, *59*(10), 1669–1679. https://doi.org/10.1175/1520-0469(2002)059<1669:lsmoan>2.0.co;2

Fuchs, Ž., Sessions, S. L., & Raymond, D. J. (2014). Mechanisms controlling the onset of simulated convectively coupled kelvin waves. *Tellus Series A Dynamic Meteorology and Oceanography*, *66*(1), 22107. https://doi.org/10.3402/tellusa.v66.22107

Hayashi, Y. (1971). A generalized method of resolving disturbances into progressive and retrogressive waves by space Fourier and time Cross-Spectral analyses. *Journal of the Meteorological Society of Japan. Ser. II*, *49*(2), 125–128. https://doi.org/10.2151/jmsj1965.49.2_125

Hersbach, H., Bell, B., Berrisford, P., Hirahara, S., Horányi, A., Muñoz-Sabater, J., et al. (2020). The ERA5 global reanalysis. *Quarterly Journal of the Royal Meteorological Society*, *64*, 29.

Hou, A. Y., Kakar, R. K., Neeck, S., Azarbarzin, A. A., Kummerow, C. D., Kojima, M., et al. (2014). The global precipitation measurement mission. *Bulletin of the American Meteorological Society*, *95*(5), 701–722. https://doi.org/10.1175/bams-d-13-00164.1

Hsiao, W.-T., Barnes, E. A., Maloney, E. D., Tulich, S. N., Dias, J., & Kiladis, G. N. (2022). Role of the tropics in state-dependent improvements of US west coast NOAA unified forecast system precipitation forecasts. *Geophysical Research Letters*, *49*(5). https://doi.org/10.1029/2021gl096447

Hsiao, W.-T., Hwang, Y.-T., Chen, Y.-J., & Kang, S. M. (2022). The role of clouds in shaping tropical pacific response pattern to extratropical thermal forcing. *Geophysical Research Letters*, *49*(11). https://doi.org/10.1029/2022gl098023

Hsiao, W.-T., Maloney, E. D., & Barnes, E. A. (2020). Investigating recent changes in MJO precipitation and circulation in multiple reanalyses. *Geophysical Research Letters*, *47*(22), e2020GL090139. https://doi.org/10.1029/2020gl090139
Hu, Q., & Randall, D. A. (1994). Low-Frequency oscillations in Radiative-Convective systems. *Journal of the Atmospheric Sciences*, *51*(8), 1089–1099. https://doi.org/10.1175/1520-0469(1994)051<1089:lfoirc>2.0.co;2
Huffman, G. J., Adler, R. F., Behrangi, A., Bolvin, D. T., Nelkin, E. J., & Ehsani, M. R. (2023). Algorithm theoretical basis document (ATBD) for global precipitation climatology project version 3.2 precipitation data. Computer software manual.
Huffman, G. J., Adler, R. F., Morrissey, M. M., Bolvin, D. T., Curtis, S., Joyce, R., et al. (2001). Global precipitation at One-Degree daily resolution from multisatellite observations. *Journal of Hydrometeorology*, *2*(1), 36–50. https://doi.org/10.1175/1525-7541(2001)002<0036:gpaodd>2.0.co;2
Inoue, K., Adames, Á. F., & Yasunaga, K. (2020). Vertical velocity profiles in convectively coupled equatorial waves and MJO: New diagnoses of vertical velocity profiles in the Wavenumber–Frequency domain. *Journal of the Atmospheric Sciences*, *77*(6), 2139–2162. https://doi.org/10.1175/jas-d-19-0209.1
Jiang, X., Adames, Á. F., Kim, D., Maloney, E. D., Lin, H., Kim, H., et al. (2020). Fifty years of research on the Madden-Julian oscillation: Recent progress, challenges, and perspectives. *Journal of Geophysical Research*, *125*(17), e2019JD030911. https://doi.org/10.1029/2019jd030911
Johnson, R. H., & Ciesielski, P. E. (2000). Rainfall and radiative heating rates from TOGA COARE atmospheric budgets. *Journal of the Atmospheric Sciences*, *57*(10), 1497–1514. https://doi.org/10.1175/1520-0469(2000)057<1497:rarhrf>2.0.co;2
Johnson, R. H., Ciesielski, P. E., Ruppert, J. H., & Katsumata, M. (2015). Sounding-Based thermodynamic budgets for DYNAMO. *Journal of the Atmospheric Sciences*, *72*(2), 598–622. https://doi.org/10.1175/jas-d-14-0202.1
Keeler, R. J., Lutz, J., & Vivekanandan, J. (2000). S-Pol: NCAR's polarimetric Doppler research radar. In *IGARSS 2000. IEEE 2000 international geoscience and remote sensing symposium. Taking the pulse of the planet: The role of remote sensing in managing the environment. proceedings (cat. No.00CH37120)* (Vol. 4, pp. 1570–1573). IEEE. https://doi.org/10.1109/igarss.2000.857275
Kiladis, G. N., Wheeler, M. C., Haertel, P. T., Straub, K. H., & Roundy, P. E. (2009). Convectively coupled equatorial waves. *Review of Geophysics*, *47*(2). https://doi.org/10.1029/2008rg000266
Kim, D., Ahn, M.-S., Kang, I.-S., & Del Genio, A. D. (2015). Role of longwave Cloud–Radiation feedback in the simulation of the Madden–Julian oscillation. *Journal of Climate*, *28*(17), 6979–6994. https://doi.org/10.1175/jcli-d-14-00767.1
Kummerow, C., Barnes, W., Kozu, T., Shiue, J., & Simpson, J. (1998). The tropical rainfall measuring mission (TRMM) sensor package. *Journal of Atmospheric and Oceanic Technology*, *15*(3), 809–817. https://doi.org/10.1175/1520-0426(1998)015<0809:ttrmmt>2.0.co;2
Lee, H.-T., Gruber, A., Ellingson, R. G., & Laszlo, I. (2007). Development of the HIRS outgoing longwave radiation climate dataset. *Journal of Atmospheric and Oceanic Technology*, *24*(12), 2029–2047. https://doi.org/10.1175/2007jtecha989.1
Lee, M.-I., Kang, I.-S., Kim, J.-K., & Mapes, B. E. (2001). Influence of cloud-radiation interaction on simulating tropical intraseasonal oscillation with an atmospheric general circulation model. *Journal of Geophysical Research*, *106*(D13), 14219–14233. https://doi.org/10.1029/2001jd900143
Li, Z., Thompson, E. J., Behrangi, A., Chen, H., & Yang, J. (2023). Performance of GPCP daily products over oceans: Evaluation using passive aquatic listeners. *Geophysical Research Letters*, *50*(11), e2023GL104310. https://doi.org/10.1029/2023gl104310
Liebmann, B., & Smith, C. A. (1996). Description of a complete (interpolated) outgoing longwave radiation dataset. *Bulletin of the American Meteorological Society*, *77*(6), 1275–1277.
Lin, J.-L., & Mapes, B. E. (2004). Radiation budget of the tropical intraseasonal oscillation. *Journal of the Atmospheric Sciences*, *61*(16), 2050–2062. https://doi.org/10.1175/1520-0469(2004)061<2050:rbotti>2.0.co;2
Ma, D., & Kuang, Z. (2011). Modulation of radiative heating by the Madden-Julian oscillation and convectively coupled kelvin waves as observed by CloudSat. *Geophysical Research Letters*, *38*(21). https://doi.org/10.1029/2011gl049734
Maloney, E. D., & Hartmann, D. L. (2000). Modulation of eastern north pacific hurricanes by the Madden–Julian oscillation. *Journal of Climate*, *13*(9), 1451–1460. https://doi.org/10.1175/1520-0442(2000)013<1451:moenph>2.0.co;2
Maloney, E. D., & Sobel, A. H. (2004). Surface fluxes and ocean coupling in the tropical intraseasonal oscillation. *Journal of Climate*, *17*(22), 4368–4386. https://doi.org/10.1175/jcli-3212.1
Mapes, B., Tulich, S., Lin, J., & Zuidema, P. (2006). The mesoscale convection life cycle: Building block or prototype for large-scale tropical waves? Dyn. *Atmosphere-Ocean*, *42*(1), 3–29. https://doi.org/10.1016/j.dynatmoce.2006.03.003
Medeiros, B., Clement, A. C., Benedict, J. J., & Zhang, B. (2021). Investigating the impact of cloud-radiative feedbacks on tropical precipitation extremes. *npj Climate and Atmospheric Science*, *4*(1), 1–10. https://doi.org/10.1038/s41612-021-00174-x
Najarian, H., & Sakaeda, N. (2023). The influence of cloud types on cloud-radiative forcing during DYNAMO/AMIE. *Journal of Geophysical Research*, *128*(8). https://doi.org/10.1029/2022jd038006
Peters, M. E., & Bretherton, C. S. (2005). A simplified model of the walker circulation with an interactive ocean mixed layer and Cloud-Radiative feedbacks. *Journal of Climate*, *18*(20), 4216–4234. https://doi.org/10.1175/jcli3534.1
Prakash, S., & Gairola, R. M. (2014). Validation of TRMM-3B42 precipitation product over the tropical indian ocean using rain gauge data from the RAMA buoy array. *Theoretical and Applied Climatology*, *115*(3), 451–460. https://doi.org/10.1007/s00704-013-0903-3
Prakash, S., Mahesh, C., & Gairola, R. M. (2013). Comparison of TRMM multi-satellite precipitation analysis (TMPA)-3B43 version 6 and 7 products with rain gauge data from ocean buoys. *Remote Sensing Letters*, *4*(7), 677–685. https://doi.org/10.1080/2150704x.2013.783248
Prigent, C. (2010). Precipitation retrieval from space: An overview. *Comptes Rendus Geoscience*, *342*(4), 380–389. https://doi.org/10.1016/j.crte.2010.01.004
Rädel, G., Mauritsen, T., Stevens, B., Dommenget, D., Matei, D., Bellomo, K., & Clement, A. (2016). Amplification of el nino by cloud longwave coupling to atmospheric circulation. *Nature*, *9*(2), 106–110. https://doi.org/10.1038/ngeo2630
Raymond, D. J. (2001). A new model of the Madden–Julian oscillation. *Journal of the Atmospheric Sciences*, *58*(18), 2807–2819. https://doi.org/10.1175/1520-0469(2001)058<2807:anmotm>2.0.co;2
Raymond, D. J., & Fuchs, Ž. (2007). Convectively coupled gravity and moisture modes in a simple atmospheric model. *Tellus*, *59*(5), 627. https://doi.org/10.1111/j.1600-0870.2007.00268.x
Raymond, D. J., Sessions, S. L., Sobel, A. H., & Fuchs, Ž. (2009). The mechanics of gross moist stability. *Journal of Advances in Modeling Earth Systems*, *1*(3). https://doi.org/10.3894/james.2009.1.9
Ruppert, J. H., Wing, A. A., Tang, X., & Duran, E. L. (2020). The critical role of cloud–infrared radiation feedback in tropical cyclone development. *Proceedings of the National Academy of Sciences*, *117*(45), 27884–27892. https://doi.org/10.1073/pnas.2013584117
Rutledge, S., Hein, P., Dolan, B., Powell, S., & Brodzik, S. (2018). NCAR s-polka radar data: DYNAMO legacy data products. Technical Report.
Schumacher, C., & Houze, R. A. (2000). Comparison of radar data from the TRMM satellite and Kwajalein oceanic validation site. *Journal of Applied Meteorology and Climatology*, *39*(12), 2151–2164. https://doi.org/10.1175/1520-0450(2001)040<2151:cordft>2.0.co;2

Sobel, A., & Maloney, E. (2012). An idealized Semi-Empirical framework for modeling the Madden–Julian oscillation. *Journal of the Atmospheric Sciences*, *69*(5), 1691–1705. https://doi.org/10.1175/jas-d-11-0118.1

Sobel, A., & Maloney, E. (2013). Moisture modes and the eastward propagation of the MJO. *Journal of the Atmospheric Sciences*, *70*(1), 187–192. https://doi.org/10.1175/jas-d-12-0189.1

Sobel, A., Wang, S., & Kim, D. (2014). Moist static energy budget of the MJO during DYNAMO. *Journal of the Atmospheric Sciences*, *71*(11), 4276–4291. https://doi.org/10.1175/jas-d-14-0052.1

Sobel, A. H., Maloney, E. D., Bellon, G., & Frierson, D. M. (2008). The role of surface heat fluxes in tropical intraseasonal oscillations. *Nature Geoscience*, *1*(10), 653–657. https://doi.org/10.1038/ngeo312

Sobel, A. H., Maloney, E. D., Bellon, G., & Frierson, D. M. (2010). Surface fluxes and tropical intraseasonal variability: A reassessment. *Journal of Advances in Modeling Earth Systems*, *2*(1). https://doi.org/10.3894/james.2010.2.2

Su, H., & David Neelin, J. (2002). Teleconnection mechanisms for tropical pacific descent anomalies during el niño. *Journal of the Atmospheric Sciences*, *59*(18), 2694–2712. https://doi.org/10.1175/1520-0469(2002)059<2694:tmftpd>2.0.co;2

Sugiyama, M. (2009). The moisture mode in the Quasi-Equilibrium tropical circulation model. Part I: Analysis based on the weak temperature gradient approximation. *Journal of the Atmospheric Sciences*, *66*(6), 1507–1523. https://doi.org/10.1175/2008jas2690.1

Takayabu, Y. N. (1994). Large-Scale cloud disturbances associated with equatorial waves. *Journal of the Meteorological Society of Japan. Sereries II*, *72*(3), 433–449. https://doi.org/10.2151/jmsj1965.72.3_433

Tseng, K.-C., Barnes, E. A., & Maloney, E. D. (2018). Prediction of the midlatitude response to strong Madden-Julian oscillation events on S2S time scales. *Geophysical Research Letters*, *45*(1), 463–470. https://doi.org/10.1002/2017gl075734

Wheeler, M., & Kiladis, G. N. (1999). Convectively coupled equatorial waves: Analysis of clouds and temperature in the Wavenumber–Frequency domain. *Journal of the Atmospheric Sciences*, *56*(3), 374–399. https://doi.org/10.1175/1520-0469(1999)056<0374:ccewao>2.0.co;2

Wheeler, M., Kiladis, G. N., & Webster, P. J. (2000). Large-Scale dynamical fields associated with convectively coupled equatorial waves. *Journal of the Atmospheric Sciences*, *57*(5), 613–640. https://doi.org/10.1175/1520-0469(2000)057<0613:lsdfaw>2.0.co;2

Wolding, B. O., & Maloney, E. D. (2015). Objective diagnostics and the Madden–Julian oscillation. Part II: Application to moist static energy and moisture budgets. *Journal of Climate*, *28*(19), 7786–7808. https://doi.org/10.1175/jcli-d-14-00689.1

Xie, P., & Arkin, P. A. (1997). Global precipitation: A 17-year monthly analysis based on gauge observations, satellite estimates, and numerical model outputs. *Bulletin of the American Meteorological Society*, *78*(11), 2539–2558. https://doi.org/10.1175/1520-0477(1997)078<2539:gpayma>2.0.co;2

Yasunaga, K., & Mapes, B. (2012). Differences between more divergent and more rotational types of convectively coupled equatorial waves. Part I: Space–Time spectral analyses. *Journal of the Atmospheric Sciences*, *69*(1), 3–16. https://doi.org/10.1175/jas-d-11-033.1

Yasunaga, K., Yokoi, S., Inoue, K., & Mapes, B. E. (2019). Space–Time spectral analysis of the moist static energy budget equation. *Journal of Climate*, *32*(2), 501–529. https://doi.org/10.1175/jcli-d-18-0334.1

Zhang, C., Adames, Á. F., Khouider, B., Wang, B., & Yang, D. (2020). Four theories of the Madden-Julian oscillation. *Review of Geophysics*, *58*(3), e2019RG000685. https://doi.org/10.1029/2019rg000685

Zurovac-Jevtić, D., Bony, S., & Emanuel, K. (2006). On the role of clouds and moisture in tropical waves: A Two-Dimensional model study. *Journal of the Atmospheric Sciences*, *63*(8), 2140–2155. https://doi.org/10.1175/jas3738.1